

Acknowledgments

We thank Erik Boehm for editorial assistance. We thank Gert Zimmer for the donation of vesicular stomatitis virus recombinant, Jay W. Hooper from the United States Army Medical Research Institute of Infectious Diseases for the plasmid encoding Puumala glycoprotein, and Jennifer Mayor for the production of recombinant vesicular stomatitis virus with Puumala virus glycoprotein. We are deeply grateful to the family for their permission to publish this article.

This work was supported by the Geneva Center for Emerging Viral Diseases and Geneva University, Faculty of Medicine.

About the Author

Dr. Vetter is an infectious diseases physician at Geneva University Hospitals and Geneva Centre for Emerging Viral Diseases, Geneva. Her research interests include emerging viral diseases.

References

1. Manigold T, Vial P. Human hantavirus infections: epidemiology, clinical features, pathogenesis and immunology. *Swiss Med Wkly*. 2014;144:w13937. <https://doi.org/10.4414/smw.2014.13937>
2. Tkachenko EA, Ishmukhametov AA, Dzagurova TK, Bernshtein AD, Morozov VG, Siniugina AA, et al. Hemorrhagic fever with renal syndrome, Russia. *Emerg Infect Dis*. 2019;25:2325–8. <https://doi.org/10.3201/eid2512.181649>
3. Kramski M, Meisel H, Klempa B, Krüger DH, Pauli G, Nitsche A. Detection and typing of human pathogenic hantaviruses by real-time reverse transcription-PCR and pyrosequencing. *Clin Chem*. 2007;53:1899–905. <https://doi.org/10.1373/clinchem.2007.093245>
4. World Health Organization. Clinical management of patients with haemorrhagic fever. 2016 [cited 2020 Sep 30]. https://apps.who.int/iris/bitstream/handle/10665/205570/9789241549608_eng.pdf
5. Alexeyev OA, Suzdaltsev AA, Verkhovtsev VN, Efratova ES, Roschupkin VI. A major outbreak of hemorrhagic fever with renal syndrome in the Samara region, European Russia. *Infection*. 1998;26:322. <https://doi.org/10.1007/BF02962264>
6. Fontana-Binard L, Schultze D, Rojanavisut BS, Krüger DH, Dollenmaier G, Zanetti G, et al. First case of nephropathia epidemica acquired in Switzerland [in French]. *Rev Med Suisse*. 2008;4:1572–5.
7. Garanina E, Martynova E, Davidyuk Y, Kabwe E, Ivanov K, Titova A, et al. Cytokine storm combined with humoral immune response defect in fatal hemorrhagic fever with renal syndrome case, Tatarstan, Russia. *Viruses*. 2019;11:601. <https://doi.org/10.3390/v11070601>
8. Mäkelä S, Mustonen J, Ala-Houhala I, Hurme M, Partanen J, Vapalahti O, et al. Human leukocyte antigen-B8-DR3 is a more important risk factor for severe Puumala hantavirus infection than the tumor necrosis factor- α (-308) G/A polymorphism. *J Infect Dis*. 2002;186:843–6. <https://doi.org/10.1086/342413>
9. Mustonen J, Partanen J, Kanerva M, Pietilä K, Vapalahti O, Pasternack A, et al. Association of HLA B27 with benign clinical course of nephropathia epidemica caused by Puumala hantavirus. *Scand J Immunol*. 1998;47:277–9. <https://doi.org/10.1046/j.1365-3083.1998.00302.x>
10. Malinin OV, Platonov AE. Insufficient efficacy and safety of intravenous ribavirin in treatment of haemorrhagic fever with renal syndrome caused by Puumala virus. *Infect Dis (Lond)*. 2017;49:514–20. <https://doi.org/10.1080/23744235.2017.1293841>

Address for correspondence: Pauline Vetter, Geneva Center for Emerging Viral Diseases, Geneva University Hospitals, 4, rue Gabrielle-Perret Gentil, 1205 Geneva, Switzerland; email: pauline.vetter@hcuge.ch; Manuel Schibler, Division of Infectious Diseases, Geneva University Hospitals, 4, rue Gabrielle Perret-Gentil, 1205 Geneva, Switzerland; email: manuel.schibler@hcuge.ch

Protective Immunity and Persistent Lung Sequelae in Domestic Cats after SARS-CoV-2 Infection

Shiho Chiba, Peter J. Halfmann, Masato Hatta, Tadashi Maemura, Shufang Fan, Tammy Armbrust, Olivia M. Swartley, LaTasha K. Crawford, Yoshihiro Kawaoka

Author affiliations: University of Wisconsin–Madison School of Veterinary Medicine, Madison, Wisconsin, USA (S. Chiba, P.J. Halfmann, M. Hatta, T. Maemura, S. Fan, T. Armbrust, O.M. Swartley, L.K. Crawford, Y. Kawaoka.); University of Tokyo Institute of Medical Science, Tokyo, Japan (Y. Kawaoka)

DOI: <https://doi.org/10.3201/eid2702.203884>

Severe acute respiratory syndrome coronavirus 2 readily transmits between domestic cats. We found that domestic cats that recover from an initial infection might be protected from reinfection. However, we found long-term persistence of inflammation and other lung lesions after infection, despite a lack of clinical symptoms and limited viral replication in the lungs.

Previous studies have demonstrated the transmissibility of severe acute respiratory syndrome coronavirus-2 (SARS-CoV-2) by direct or indirect contact between domestic cats (1,2). Given the

close relationship between cats and humans, further characterization of the biology of SARS-CoV-2 in cats is warranted.

We inoculated domestic cats with SARS-CoV-2, and on postinfection days 3, 6, and 10, sampled organs to titrate virus (Appendix Figure 1, <https://wwwnc.cdc.gov/EID/article/27/2/20-3884-App1.pdf>). In plaque-forming assays in VeroE6/TMPRSS2 cells, infectious viruses were detected in the nasal turbinates and trachea of all animals on day 3, and most on day 6, whereas virus detection in the lungs was limited on day 3 and absent on day 6 (Appendix Figure 2, panel A). These results suggest that the virus replicated efficiently in upper respiratory organs, which might contribute to its high transmissibility among cats. Infectious virus was cleared from the upper and lower respiratory organs by day 10 (Appendix Figure 2, panel A). No animal showed any signs of respiratory illness during the study (Appendix Figure 3). Infectious virus was not detected (detection limit 10 pfu/g of tissue) in other examined organs (e.g., brain, liver, spleen, kidney, small and large intestine, heart, and eyelids). Viral antigen was detected in nasal turbinates and trachea but was sparse within the lungs at day 3 (Appendix Figure 4).

We conducted histopathologic examination of the lungs, trachea, and nasal turbinates. Lymphocytic inflammation within the tracheal submucosa was

present on days 3 to 10, whereas lymphocytic to mixed inflammation in the nasal cavity was more severe on days 3 and 6 but minimal on day 10. In lungs, moderate lesions persisted despite clearance of virus. On day 3, we observed mild bronchitis with lymphoid hyperplasia, moderate to severe histiocytic bronchiolitis with partial to complete occlusion of lumina, and moderate to severe thickening of alveolar septa (Appendix Figure 2, panel B; Appendix Figures 4, 5). Interstitial inflammatory infiltrate decreased significantly over time ($p = 0.0012$, $F = 34.70$, by 1-way analysis of variance) (Appendix Figure 2, panel C); however, by day 10, alveolar septa remained thickened (Appendix Figure 5). Bronchiolitis remained with partial occlusion of bronchioles, even in regions with minimal alveolar lesions (Appendix Figure 2, panel B).

Because SARS-CoV-2 did not cause acute lethal respiratory disease in the cats in our study, cats are a compelling animal model for studying the long-term effects of nonfatal infections. Cats were infected with SARS-CoV-2 and euthanized at postinfection day 28 (Appendix Figure 6, 7). Persistent lung lesions were observed 28 days after infection, including histiocytic bronchiolitis with luminal plugs and thickened alveolar septa, similar to lesions observed on day 10 but with more chronic features such as peribronchiolar fibrosis and vascular

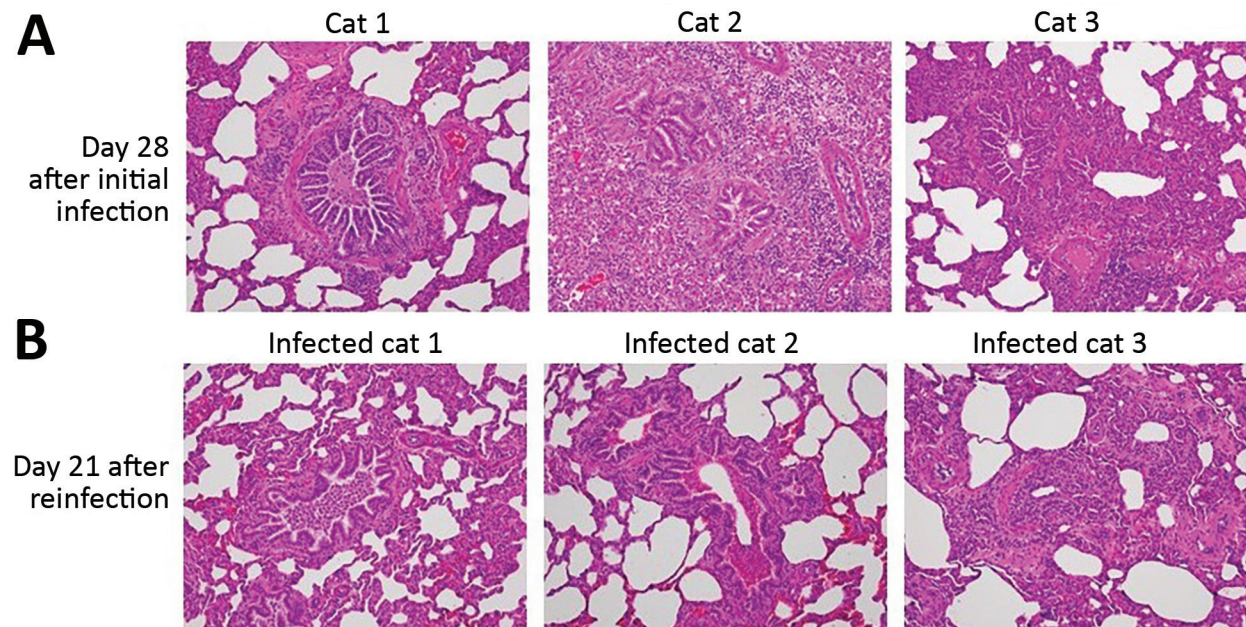


Figure 1. Comparison of histopathology between cats on day 28 after initial infection with severe acute respiratory syndrome coronavirus 2 and on day 21 after reinfection. Bronchioles and alveoli of cats (cats 1–3 in Appendix Figure 6; <https://wwwnc.cdc.gov/EID/article/27/1/20-3884-App1.pdf>) on day 28 after initial infection (A) and those of cats (infected cats 1–3 in Appendix Figure 6, upper half) on day 21 after reinfection (49 days after the initial infection) (B); original magnification 20 \times . Cats from both groups showed histiocytic bronchiolitis with occlusive plugs, peribronchiolar fibrosis, and thickening of alveolar septa. Mild acute hemorrhage was detected in affected and less affected regions of the lung on day 21 after reinfection, with a trend toward an increase compared with day 28 (severity score $1.8 \pm \text{SEM } 0.8$ on day 21 vs. $0.3 \pm \text{SEM } 0.2$ on day 28; $p = 0.187$ by unpaired *t*-test).

proliferation within the thickened interstitium. We observed a notable dearth of fibrosis within alveolar septa, in contrast to what has been reported for humans with severe acute respiratory syndrome or Middle East respiratory syndrome (3,4). One cat had severe pneumonia with fibrin in alveolar spaces and endothelialitis (Appendix Figure 8), similar to what has been reported in humans with fatal coronavirus disease (5), although this cat did not show any respiratory signs.

To determine whether previous infection provides protection from future potential infection by SARS-CoV-2, we performed a reinfection study with 2 groups of cats. We previously reported that SARS-CoV-2 was transmitted from cats inoculated with the virus to cohoused, naive cats (1). In the previous study, the 3 cats that had been inoculated with SARS-CoV-2, whose nasal swabs were virus-negative on day 6 or 7 after the initial infection (1), were rein-

oculated with the same virus 4 weeks after the initial infection (Figure 1; Figure 2, panel A). No infectious virus was detected in the nasal or rectal swabs after reinfection, suggesting that the animals were protected from reinfection. These cats were euthanized at 21 days after reinfection (49 days after the initial infection), and tissue was submitted for histopathologic examination. The reinfection group showed lesions that were comparable with lung lesions observed on day 28 but with less severe thickening of alveolar septa ($p = 0.041$, by unpaired *t*-test) (Figure 1; Figure 2 panel B). The 3 cats in the other group, which recovered from infection that was transmitted by contact with virus-inoculated cats, were reinfected with the virus at ≈ 4 weeks (29–32 days) after transmission. On day 3 after reinfection, organs were harvested; infectious virus was not detected (detection limit 10 pfu/g of tissue) in respiratory organs or other organs

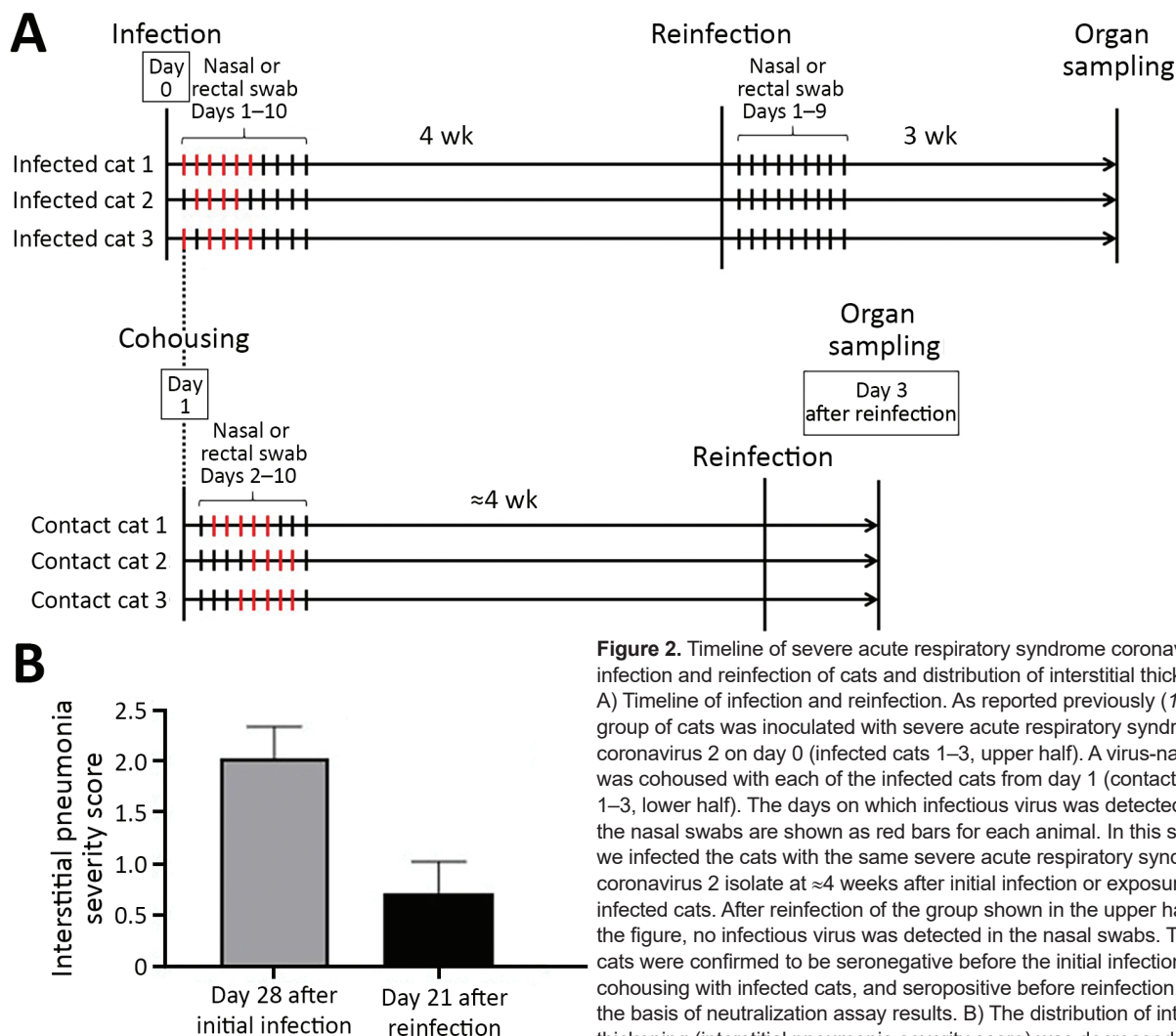


Figure 2. Timeline of severe acute respiratory syndrome coronavirus 2 infection and reinfection of cats and distribution of interstitial thickening. A) Timeline of infection and reinfection. As reported previously (1), a group of cats was inoculated with severe acute respiratory syndrome coronavirus 2 on day 0 (infected cats 1–3, upper half). A virus-naive cat was cohoused with each of the infected cats from day 1 (contact cats 1–3, lower half). The days on which infectious virus was detected in the nasal swabs are shown as red bars for each animal. In this study, we infected the cats with the same severe acute respiratory syndrome coronavirus 2 isolate at ≈ 4 weeks after initial infection or exposure to infected cats. After reinfection of the group shown in the upper half of the figure, no infectious virus was detected in the nasal swabs. The cats were confirmed to be seronegative before the initial infection or cohousing with infected cats, and seropositive before reinfection, on the basis of neutralization assay results. B) The distribution of interstitial thickening (interstitial pneumonia severity score) was decreased on day 21 after reinfection compared with day 28 ($p = 0.041$ by unpaired *t*-test).

analyzed (e.g., brain, liver, spleen, kidney, small and large intestine, heart, and eyelids). These results suggest that virus infection by natural transmission between cats, as well as by experimental inoculation, induces protective immunity against a second SARS-CoV-2 infection.

In conclusion, SARS-CoV-2 replicated effectively in the upper respiratory tract in cats, and infectious virus was cleared from the lungs within 6 days of infection; however, histopathologic examination demonstrated chronic lung sequelae in cats even a month after viral clearance. After initial infection with SARS-CoV-2, cats were protected from reinfection, with no virus replication in respiratory organs and no additional lung damage.

Acknowledgment

We thank Gillian McLellan for the cats used in this study and Sue Watson for scientific editing. We would also like to thank Angela Brice and Olga Gonzalez for sharing their expertise with our pathologists during consultation as well as Amanda Novak, Emily Tran, and Sara Stuedemann for their technical support.

This research was supported by the Center for Research on Influenza Pathogenesis, funded by the National Institutes of Allergy and Infectious Diseases, National Institutes of Health (grant no. HHSN272201400008C awarded to Y.K.); the Research Program on Emerging and Re-emerging Infectious Disease from Japan Agency for Medical Research and Development (AMED) (grant no. JP19fk0108113 awarded to Y.K.); the Japan Initiative for Global Research Network on Infectious Diseases from AMED (grant no. JP19fm0108006 awarded to Y.K.); the Japan Program for Infectious Diseases Research and Infrastructure from AMED (grant no. JP20wm0125002 to Y.K.); and a University of Wisconsin K12 Career Development Award from the National Institute of Diabetes and Digestive and Kidney Diseases (grant no. K12DK100022 awarded to L.K.C.).

About the Author

Dr. Chiba is a molecular virologist at the Influenza Research Institute at the University of Wisconsin–Madison, with a background in innate immunity studies and structural biology. Her primary research interests include mechanisms of virus infection, virus antigenicity, and host immune responses.

References

1. Halfmann PJ, Hatta M, Chiba S, Maemura T, Fan S, Takeda M, et al. Transmission of SARS-CoV-2 in domestic cats. *N Engl J Med*. 2020;383:592–4. <https://doi.org/10.1056/NEJMc2013400>
2. Shi J, Wen Z, Zhong G, Yang H, Wang C, Huang B, et al. Susceptibility of ferrets, cats, dogs, and other domesticated animals to SARS-coronavirus 2. *Science*. 2020;368:1016–20. <https://doi.org/10.1126/science.abb7015>
3. Cheung OY, Chan JW, Ng CK, Koo CK. The spectrum of pathological changes in severe acute respiratory syndrome (SARS). *Histopathology*. 2004;45:119–24. <https://doi.org/10.1111/j.1365-2559.2004.01926.x>
4. Das KM, Lee EY, Singh R, Enani MA, Al Dossari K, Van Gorkom K, et al. Follow-up chest radiographic findings in patients with MERS-CoV after recovery. *Indian J Radiol Imaging*. 2017;27:342–9. https://doi.org/10.4103/ijri.IJRI_469_16
5. Ackermann M, Verleden SE, Kuehnel M, Haverich A, Welte T, Laenger F, et al. Pulmonary vascular endothelialitis, thrombosis, and angiogenesis in Covid-19. *N Engl J Med*. 2020;383:120–8. <https://doi.org/10.1056/NEJMoa2015432>

Address for correspondence: Yoshihiro Kawaoka, 575 Science Dr, Madison, Wisconsin 53711, USA; email: yoshihiro.kawaoka@wisc.edu; or LaTasha K. Crawford, 2015 Linden Dr, Madison, Wisconsin 53706, USA; email: lk Crawford@wisc.edu

Long-Term Humoral Immune Response in Persons with Asymptomatic or Mild SARS-CoV-2 Infection, Vietnam

Huynh Kim Mai, Nguyen Bao Trieu, Trinh Hoang Long, Hoang Tien Thanh, Nguyen Dinh Luong, Le Xuan Huy, Lam Anh Nguyet, Dinh Nguyen Huy Man, Danielle E. Anderson, Tran Tan Thanh, Nguyen Van Vinh Chau, Guy Thwaites, Lin-Fa Wang, Le Van Tan, Do Thai Hung

Author affiliations: Pasteur Institute, Nha Trang City, Vietnam (H.K. Mai, N.B. Trieu, T.H. Long, H.T. Thanh, N.D. Luong, L.X. Huy, D.T. Hung); Oxford University Clinical Research Unit, Ho Chi Minh City, Vietnam (L.A. Nguyet, T.T. Thanh, G. Thwaites, L.V. Tan); Hospital for Tropical Diseases, Ho Chi Minh City (D.N.H. Man, N.V.V. Chau); Duke-NUS Medical School, Singapore (D.E. Anderson, L.-F. Wang); Centre for Tropical Medicine and Global Health, Nuffield Department of Medicine, University of Oxford, Oxford, UK (G. Thwaites); SingHealth Duke-NUS Global Health Institute, Singapore (L.-F. Wang)

DOI: <https://doi.org/10.3201/eid2702.204226>

Protective Immunity and Persistent Lung Sequelae in Domestic Cats after SARS-CoV-2 Infection

Appendix

Materials and Methods

Virus

The SARS-CoV-2 isolate UT-NCGM02/Human/2020/Tokyo was isolated in VeroE6 and passaged twice on VeroE6 cells.

Cells

Vero E6/TMPRSS2 cells were obtained from the National Institute of Infectious Diseases, Japan. Cells were maintained in Dulbecco's modified Eagle's medium (DMEM) containing 10% fetal bovine serum (FBS) and antibiotic/antimycotic (anti/anti) solution as well as G418 (1 mg/ml).

Cats

Animal studies were approved and performed in accordance with the Animal Care and Use Committee guidelines at the University of Wisconsin-Madison. The male and female domestic cats (15–18-week-old) used in these transmission and re-infection studies were specific-pathogen-free animals from a research colony maintained at the University of Wisconsin-Madison. The male domestic cats (19-week-old) used in the virus replication and pathology study were purchased from Marshall BioResources. All animals were housed with 48%–65% humidity at 23°C, and with at least 15.2 air exchanges per hour. Weight and body temperature were recorded daily.

Experimental Infection of Cats

Under ketamine and dexdomitor anesthesia, cats were inoculated with 5.2×10^5 plaque-forming units (PFU) of SARS-CoV-2 via a combination of inoculation routes for every animal (nasal [100 μ l per nare], tracheal [500 μ l], oral [500 μ l], and ocular [inoculation in the eyes; 50

µl per eye]). To reverse the effects of the anesthesia, antisedan was administered to the animals after completion of the inoculation. No control (mock-infected) cats were included in this study.

Swab Sample Collection

In the re-infection study, nasal and rectal swabs were collected daily after re-infection (Days 1–9). The swabs were soaked in DMEM for seconds before obtaining the nasal and rectal samples. After collection, the swabs were placed in a tube containing 1.0 ml of DMEM containing anti/anti solution and vortexed for 1 minute in preparation for the virus titration assay.

Virus Titration Assay

Confluent Vero E6/TMPRSS2 cells in 12-well plates were infected with 100 µl of undiluted or 10-fold dilutions (10^{-1} to 10^{-5}) of the homogenized organ samples or the nasal or rectal swab samples. After a 30-minute incubation, the virus inoculum was removed, the cells were washed once, and then overlaid with 1% methylcellulose solution in DMEM with 5% FBS. The plates were incubated for 3 days, and then the cells were fixed and stained with 20% methanol and crystal violet to count the plaques.

Pathological Examination

Cats were euthanized and tissues collected using standard biocontainment protocols. All cats were deeply anesthetized with the combination of ketamine and dexdomitor, and euthanized by exsanguination by bleeding from cervical artery. Macroscopic lesions were detected at all time points in lungs (data not shown). Lungs were infused with 10% formalin phosphate buffer solution via the trachea before immersion fixation in formalin along with trachea, a segment of the skull containing the nasal cavity, and other tissues. Lungs were trimmed to generate 6 representative sections of lung, including one section of the cranial and caudal segments of the left lung lobe and one from each remaining lobe. Each section included at least one grossly visible bronchus. The trachea was trimmed to generate a single cross section and the skull was trimmed to obtain a single cross section containing bilateral nasal turbinates. Standard paraffin embedded tissues were sectioned to generate slides stained with hematoxylin and eosin (HE). Selected slides were also stained with Gomori's trichrome stain. After initial evaluation, each section of lung, trachea, and nasal cavity was scored by one of two board-certified veterinary pathologists who were both blinded to the identity of the animals and experimental groups. The distribution of rhinitis, tracheitis, and thickened alveolar septa beyond 2x normal was scored on a

scale of 1 to 5 with 1 affecting <5%, 2 affecting 5%–20%, 3 affecting 20%–50%, 4 affecting 50%–80%, and 5 affecting >80% of the evaluated tissue. A score of 0–5, where 0 = absent, 1 = minimal, 2 = mild, 3 = moderate, 4 = marked, 5 = severe or fulminating, was given for other lesions including bronchitis, bronchiolitis with occlusive plugs, interstitial inflammatory infiltrate, and hemorrhage. Inflammation was scored based on the degree of inflammatory infiltrate; the type of inflammatory infiltrate was characterized separately, based on the predominant inflammatory cell types. Megakaryocytes were enumerated across ten 20X fields, each measuring 800 microns in diameter. For the lung, scores were averaged across lung sections for each individual, then averaged across each experimental group. The nasal turbinates and trachea were only evaluated on day 3, 6, and 10 post-infection. Statistical analysis was conducted using Prism 8 software (GraphPad Software, San Diego, CA). Corrections for multiple t-test comparisons were not used when the comparisons were complementary.

Immunofluorescent Staining

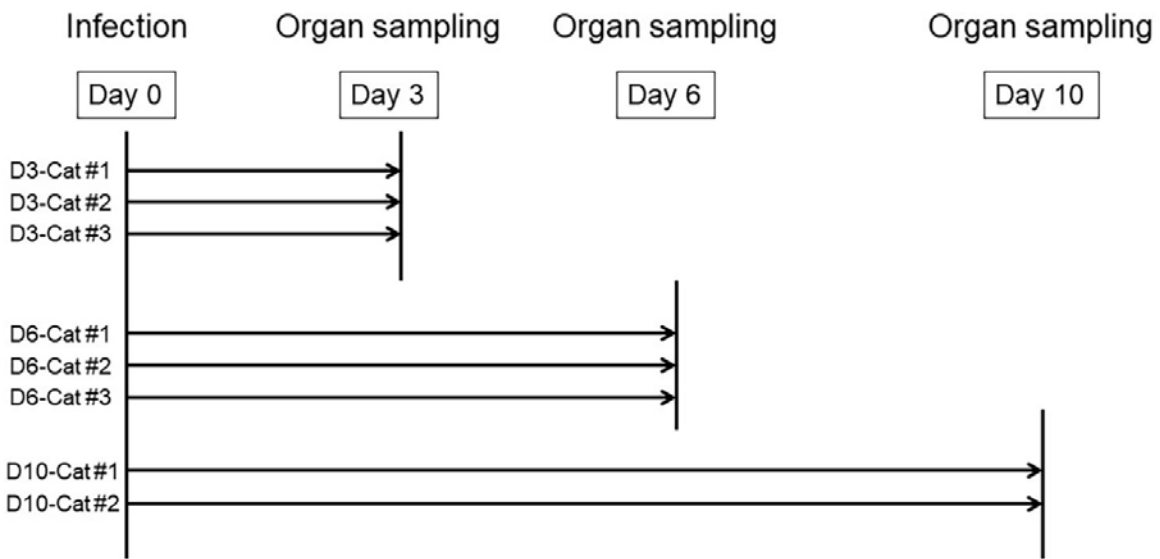
A representative tissue section from a cat in each major experimental group was selected. Sections were deparaffinized and then subject to heat-induced antigen retrieval in pH 6 citrate-buffer followed by a standard immunofluorescent staining protocol to detect SARS-CoV viral antigen in tissue sections. This included block in 5% normal donkey serum in 0.1% triton-X in phosphate buffered saline blocking solution, overnight room temperature incubation in 1:500 Rabbit polyclonal SARS Nucleocapsid protein antibody (Novus Biologicals, NB100–56576), 2 hour incubation in 1:500 Donkey anti-Rabbit Alexa 647 secondary antibody (Jackson ImmunoResearch Labs, A31573), quenching of tissue autofluorescence with TrueVIEW quenching kit (Vector Labs, SP-8400–15), and several buffer washes between each step. Epifluorescent images were acquired on Thunder 3D Tissue microscope (Leica Microsystems) using LAS X software (Leica Microsystems).

Biosafety Statement

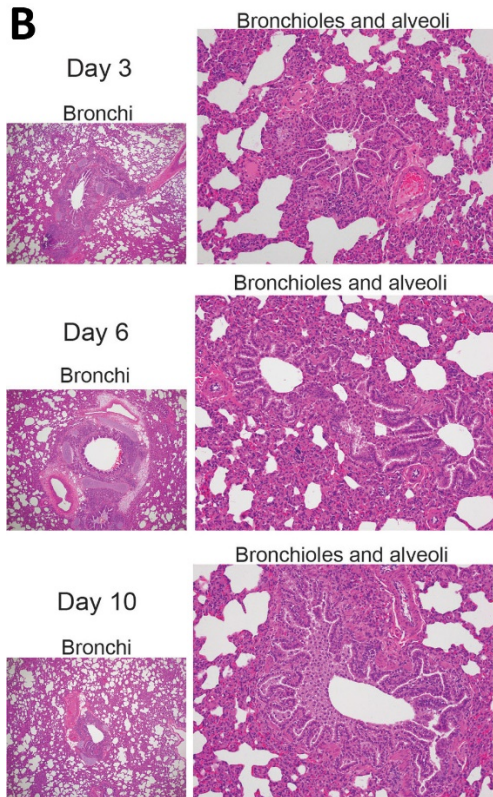
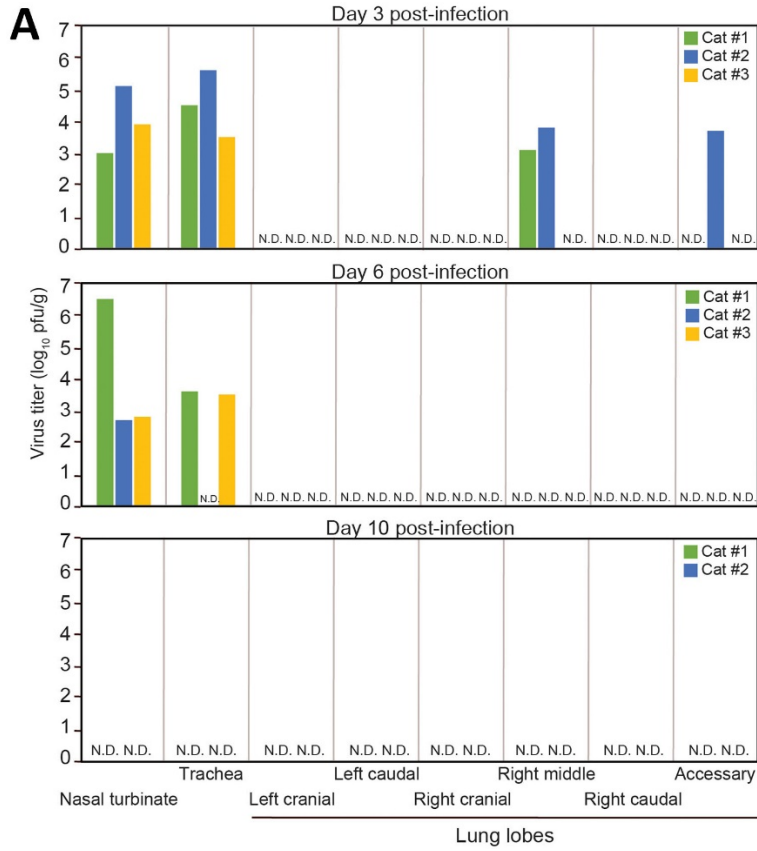
The recombinant DNA protocol for the use of the virus was approved by the University of Wisconsin-Madison's Institutional Biosafety Committee. The cat transmission study with SARS-CoV-2 was performed in biosafety level 3 agriculture (BSL-3Ag) laboratories at the Influenza Research Institute, the University of Wisconsin-Madison. These laboratories are approved for such use by the Centers for Disease Control and Prevention. The BSL-3Ag facility

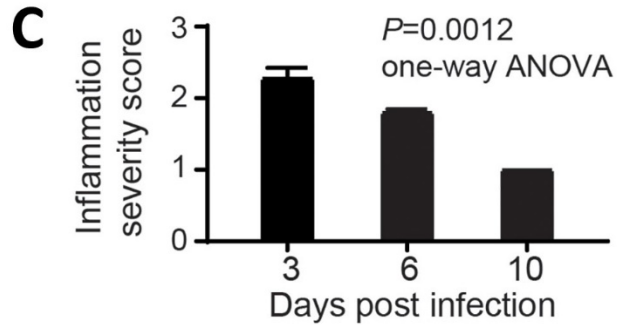
used was designed to exceed the standards outlined in *Biosafety in Microbiological and Biomedical Laboratories* (5th edition).

Features of the BSL-3Ag facility include controlled access, entry/exit through a shower change room, effluent decontamination, negative air-pressure, double-door autoclaves, gas decontamination ports, HEPA-filtered supply and double-HEPA-filtered exhaust air, double-gasketed watertight and airtight seals, and airtight dampers on all ductwork. The structure of the BSL-3Ag facility is pressure-decay tested regularly.

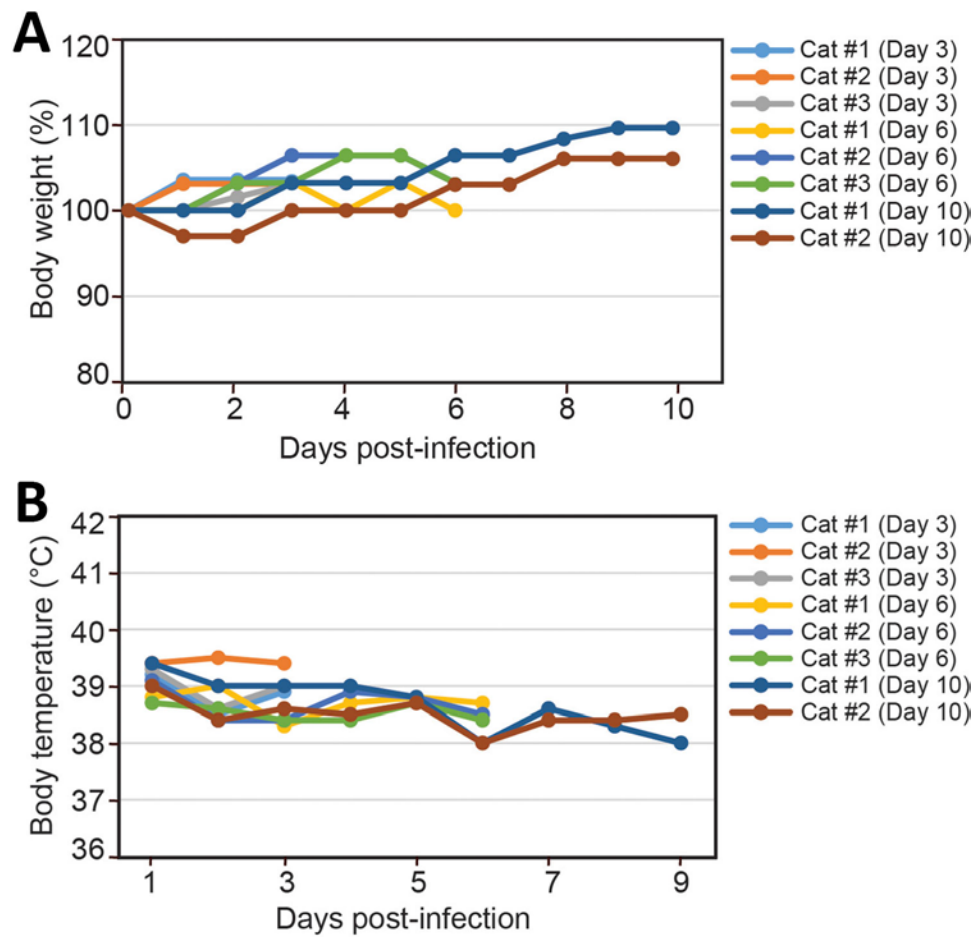


Appendix Figure 1. Timeline of cat infection and organ sampling in this study.

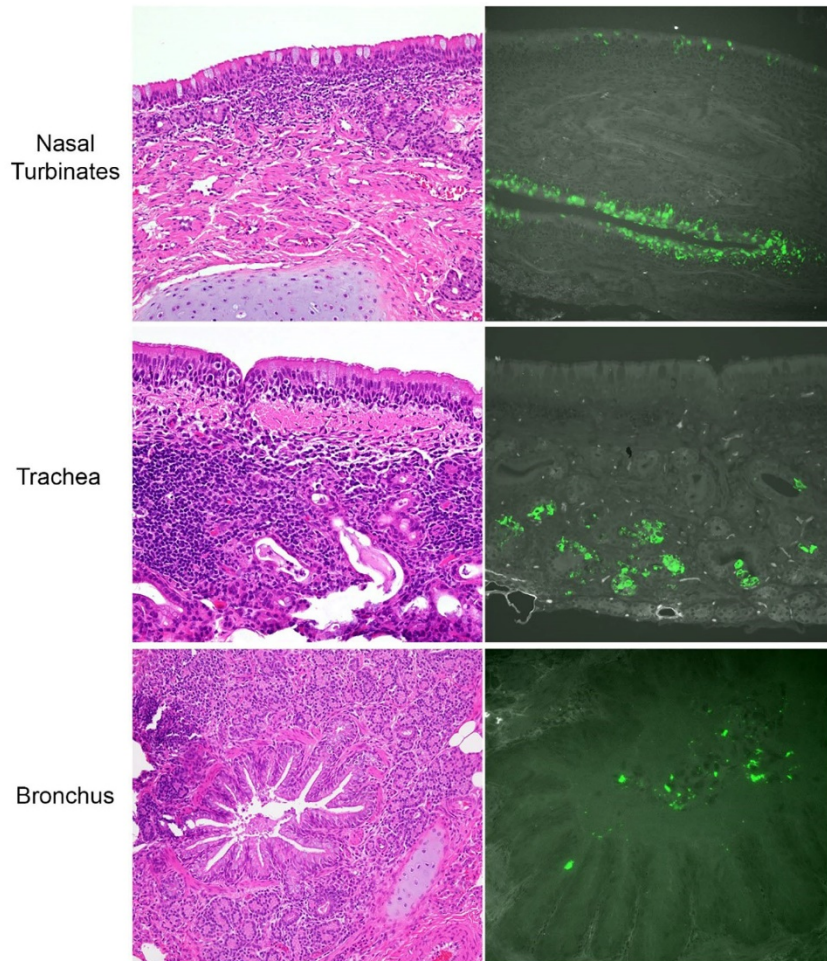




Appendix Figure 2. Replication and pathogenicity of SARS-CoV-2 in cat respiratory organs. (A) Cats were inoculated with SARS-CoV-2. On Days 3, 6, and 10 post-infection, their organs were collected to assess infectious virus titers. N.D., infectious virus not detected (<10 pfu/g). (B) Typical images of hematoxylin and eosin (HE)-stained bronchi, bronchioles, and alveoli on days 3, 6, and 10 post-infection. Bronchitis was mild with lymphoid hyperplasia that diminished over time and sloughed epithelial cells in the lumen at day 3 (see Appendix Figure 4) were minimal to absent at day 6 and day 10. Bronchiolitis was persistent throughout all examined time points with partial and, rarely, complete occlusion of bronchiolar lumens by sheets of epithelioid-like macrophages that were occasionally continuous with macrophages in the bronchiole walls and peribronchiolar connective tissue. Thickening of alveolar septa was likewise persistent (see Appendix Figure 5). (C) Interstitial inflammatory infiltrate significantly decreased in lungs over time, as indicated by the inflammation severity score.

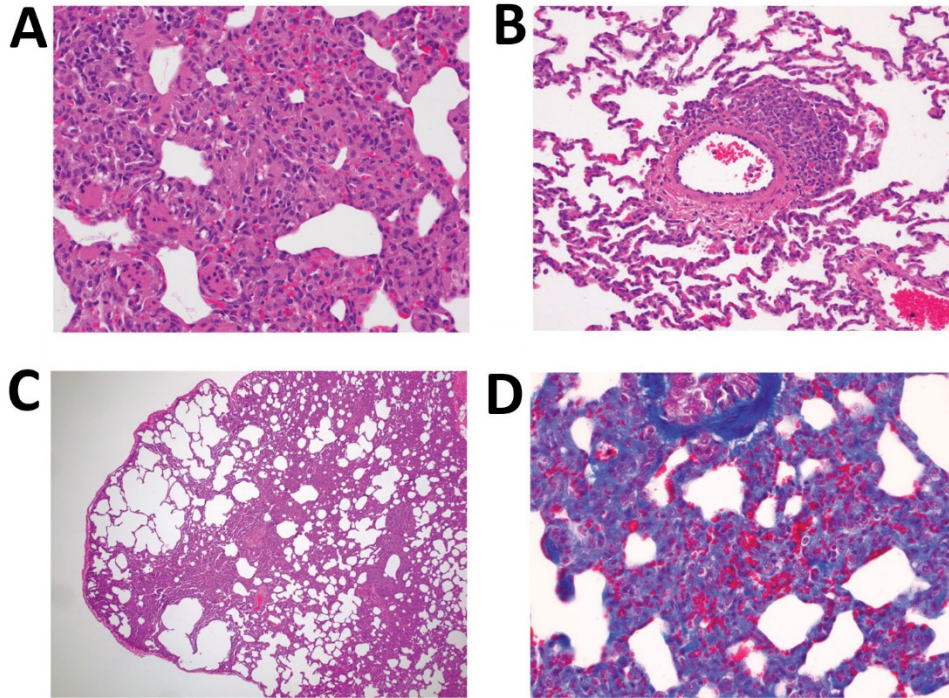


Appendix Figure 3. Changes in bodyweight (A) and body temperature (B) of SARS-CoV-2-infected cats euthanized on day 3, 6, or 10 post-infection.

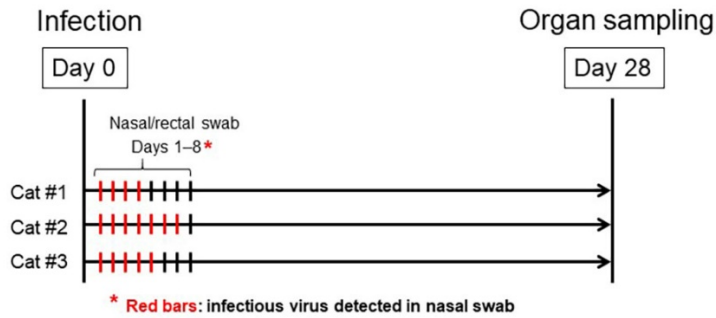


Appendix Figure 4. At day 3, viral antigen was detected in regions corresponding to lesions of the nasal turbinates and trachea but was not detected in lesions in the lung. In the nasal cavity, inflammation was in the superficial submucosa and frequently infiltrated the epithelium (top panel, left). Viral antigen was detected in the nasal epithelium, within cells suspected to be olfactory epithelial cells (top panel, right). In the trachea, inflammation was deeper within the submucosa surrounding and occasionally effacing submucosal glands (middle panel, left). Viral antigen in the trachea was detected within submucosal glandular epithelium (middle panel, right). Similar distribution and character of inflammation was present in the trachea at day 6 and day 10, while inflammation trended toward a decrease to minimal by day 10 in the nasal turbinates (data not shown). In the lung, bronchitis consisted of mild inflammation within submucosal glands along with lymphoid hyperplasia (lower, left). Viral antigen was sparse in the lung and was only found in sloughed epithelial cells and debris in the lumen of bronchi and scattered along the apical surface of the bronchial epithelium (lower panel, right). Viral antigen was not detected in the bronchioles or alveoli. HE images on the left, 20X magnification. On the right, immunofluorescent staining for viral antigen was pseudocolored green during image acquisition with a far red light source and merged with a greyscale image of autofluorescence acquired with GFP light source; nasal and trachea 20X magnification, bronchus 40X magnification.

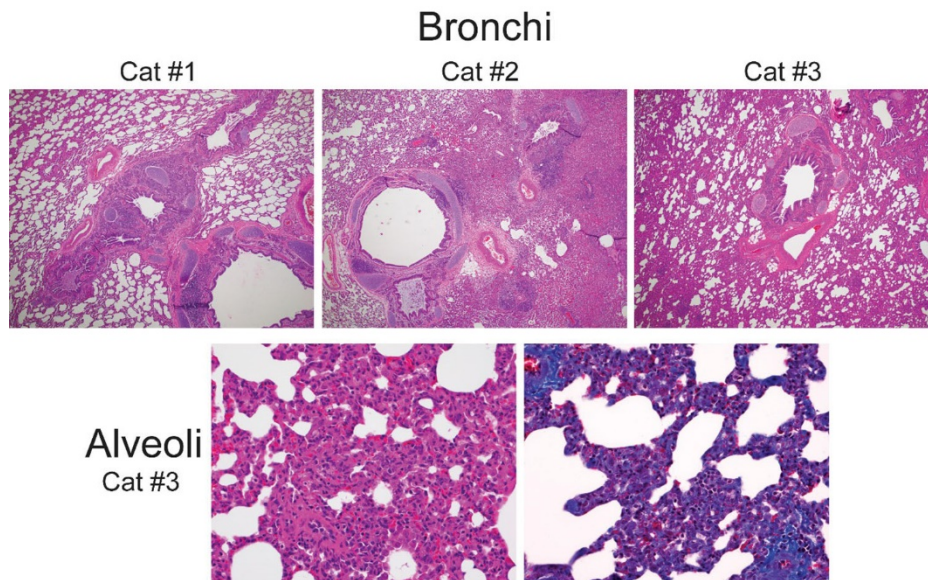
Alveolar Interstitium



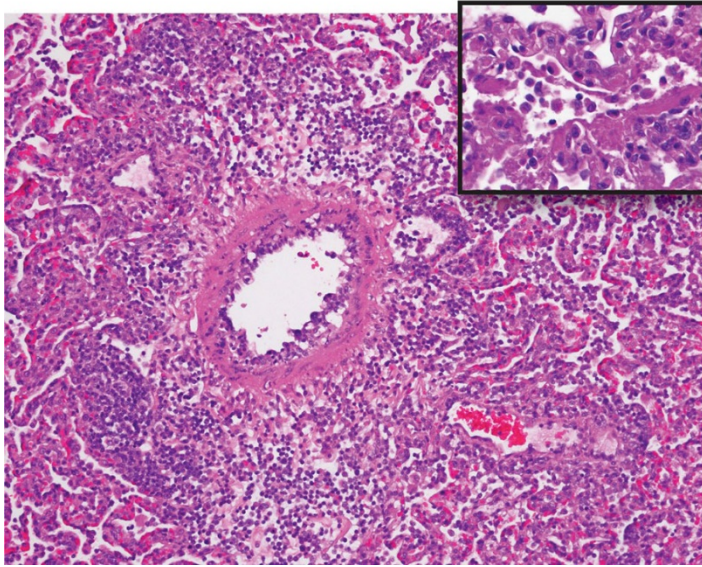
Appendix Figure 5. The alveolar interstitium is thickened after SARS-CoV-2 infection. (A) At day 3, in patchy to coalescing regions of the lung, the alveolar septa are thickened by a variable combination of type II pneumocytes, abundant macrophages, moderate numbers of neutrophils, and fewer lymphocytes, along with stromal cells that are suspected to be vascular precursors. Respiratory bronchioles were often lined by attenuated epithelium as seen in the lower left aspect of the image. Intravascular megakaryocytes (not shown) decreased slightly over time (ranging from 8.0 to 3.4 per ten 20X fields, $p = 0.189$ one way ANOVA). HE, 40X magnification. (B) Multifocal perivascular lymphocytic nodules admixed with scattered macrophages were present, sometimes in lesser affected areas of the section. Perivascular lymphocytic nodules in more severely affected regions occasionally extend into and thicken adjacent alveolar septa (not shown). Vascular endothelium was diffusely reactive at all timepoints examined, often ranging from plump to vacuolated. HE, 20X magnification. Images in (A) and (B) are from day 3, Cat #3. (C) By day 10, distention of alveolar spaces was seen in some regions adjacent to patchy atelectasis while other regions of the lung showed thickened alveolar septa with a notable lack of fibrosis. HE 4X magnification. (D) On trichrome stain, mature collagen and smooth muscle stain dark blue, while dark blue is notably sparse to absent within the thickened interstitium, confirming that fibrosis is minimal. Gomori trichrome stain, 40X magnification. Images in (C) and (D) are from day 10, Cat #1.



Appendix Figure 6. Timeline of cat infection and organ sampling in this study. On days 1–8 post-infection, nasal and rectal swabs were taken from the cats and infectious virus was titrated by performing plaque assays. The days on which infectious virus was detected in the nasal swabs are shown as red bars for each animal. The animals were confirmed to be seronegative by performing a neutralization assay before they were infected.



Appendix Figure 7. Histopathology of the lungs of cats at 28 days post-infection (Cats #1–3 in Appendix Figure 6). Histopathology was consistent with that seen at 10 days post-infection with more chronicity, including multifocal histiocytic bronchiolitis with luminal plugs and regional thickening alveolar septa (top panel, 4X magnification). Alveolar septa were thickened by macrophages, lymphocytes, and fewer neutrophils and plasma cells with increased stromal cells suggestive of vascular proliferation (lower panel, 40X magnification). Gomori trichrome stain, wherein mature collagen and smooth muscle stains dark blue, demonstrates mature collagen surrounding medium caliber vessels, foci of smooth muscle within the tips of alveolar septa and in respiratory bronchioles, and a notable lack of fibrosis within the thickened interstitium (lower panel, right, 40X magnification). Lung lesions were particularly severe in Cat #2 (see Appendix Figure 8).



Appendix Figure 8. The lung lesions of one cat at day 28 was particularly severe. Lung pathology in a single cat (Cat #2 in Appendix Figures 6 and 7) was particularly severe with endothelialitis (vasculitis), severe perivascular inflammation and edema, and alveolar collapse with macrophages, lymphocytes, plasma cells and lower numbers of neutrophils within alveolar spaces. HE, 20X magnification. Inset shows PAS stain of accumulation of fibrin and cellular debris along with inflammatory cells within alveolar spaces. PAS stain, 40X magnification.